Sensors and Actuators A 326 (2021) 112682

Contents lists available at ScienceDirect

Sensors and Actuators A: Physical

journal homepage: www.elsevier.com/locate/sna

Comparison of three types of fiber optic sensors for temperature monitoring in a groundwater flow simulator

Sandra Drusová [a,b,*], Wiecher Bakx [a,c], Pieter J. Doornenbal [d], R. Martijn Wagterveld [a], Victor F. Bense [e], Herman L. Offerhaus [b]

[a] Wetsus, European Centre of Excellence for Sustainable Water Technology, Oostergoweg 9, 8911 MA Leeuwarden, The Netherlands
[b] Optical Sciences, University of Twente, Hallenweg 23, 7522 NH Enschede, The Netherlands
[c] Arcadis, Beaulieustraat 22, 6814 DV Arnhem, The Netherlands
[d] Department of Subsurface and Groundwater Systems, Deltares, Utrecht, The Netherlands
[e] Hydrology and Quantitative Water Management, Department of Environmental Sciences, Wageningen University, The Netherlands

ARTICLE INFO

Article history:
Received 1 May 2020
Received in revised form 8 January 2021
Accepted 8 March 2021
Available online 17 March 2021

Keywords:
Distributed temperature sensing
Fiber Bragg grating
Continuous fiber Bragg grating
Groundwater temperature
Strain
Packaging

ABSTRACT

Different fiber optic sensors have been used for groundwater temperature monitoring and the question is which one to choose for a particular study. In the field conditions it is sometimes difficult to determine how much error is introduced by the sensor placement technique, packaging or cross-sensitivity between temperature and strain. These factors were studied in a laboratory groundwater simulator during a heat tracing experiment. The performance of three fiber optic technologies was evaluated – distributed temperature sensing, fiber Bragg gratings and continuous fiber Bragg gratings. All sensors had comparable accuracy of around 0.2 °C and resolution smaller than 0.1 °C. Therefore, factors which need to be considered when choosing a sensor for groundwater temperature monitoring are spatial resolution, sampling frequency and possibility to measure absolute/relative temperature. The experiment also showed that strain effects can be introduced even when fibers have a loose tube packaging.

1. Introduction

Monitoring groundwater temperature is important to investigate subsurface processes and assess the impact of groundwater usage on the environment [1]. Temperature changes influence groundwater flow [2] and water quality [3,4] because groundwater density, viscosity and solubility of ions are all temperature-dependent properties. Since heat is transported by groundwater flow, groundwater temperature is used to determine aquifer recharge and discharge [5], surface water [6] and fracture inflows [7]. Groundwater temperature distribution is needed to improve the efficiency of Aquifer Thermal Energy Storage (ATES) systems [8] and identify the leakage at remediation and mining sites [9,10].

A common way of measuring groundwater temperature is by using thermometers, thermocouples, or waterproof temperature loggers inside boreholes. All of these devices are discrete point sensors with separate wire connections to the surface so that the spatial resolution of the collected temperature data is determined by the number of sensors installed over a certain distance. Installing many traditional sensors is labor intensive and technically difficult. In recent years, fiber optic sensors opened up the possibility to study groundwater temperature with higher spatial resolution than with traditional sensors [11]. A single optical fiber can provide multiple measurement points or intervals along its length. There are several fiber optic sensing technologies available on the market. In general, they can be divided into two categories – multiplexed and distributed sensors [12].

Multiplexed sensors contain isolated measurement points inside a fiber arranged in a linear array. An example of sensors that can be multiplexed is **fiber Bragg gratings (FBGs)**. A single FBG sensor is a periodic modulation of the refractive index over a short distance that was created by a UV laser inside the photosensitive fiber core. This distance is generally less than 10 mm. The grating created in this manner acts like a mirror for a light with wavelength λ_B that matches the Bragg condition [13]:

$$\lambda_B = 2n_{eff}\Lambda \quad (1)$$

where n_{eff} is the effective refractive index of the fiber and Λ is the grating period. The grating period can be changed by applying

* Corresponding author.
E-mail address: s.drusova@utwente.nl (S. Drusová).

https://doi.org/10.1016/j.sna.2021.112682

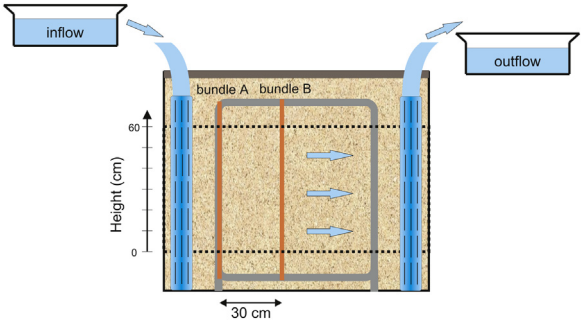

Fig. 1. The cross-section of the groundwater flow simulator Heat maps in the results were created from all sensors located in the central section of the tank (with boundaries indicated by a dashed line).

strain or varying the temperature of the fiber, causing a shift in the reflected wavelength.

Distributed sensors measure temperature and strain over the entire length of the optical fiber, where the fiber itself is a sensing element. An example of a distributed sensor is **continuous fiber Bragg grating (CFBG)**. A CFBG has a continuous refractive index modulation along the length offering a continuous coverage. Other types of distributed sensors are based on scattering phenomena in the glass [14]. Raman scattering is the underlying principle of the **distributed temperature sensing (DTS)** method. DTS has the advantage that it is not simultaneously dependent on strain. Light scattering in a fiber is a random process with a very low intensity; therefore, measurements require a longer time and averaging. Grating structures give reflected light with much higher intensity than scattered light, and measurements can be acquired at higher frequencies.

DTS is the most widely applied fiber optic technology for groundwater temperature sensing. DTS was used to study the interaction between groundwater and surface water [15,16], groundwater flow in boreholes [17,18], and aquifers [19,20]. FBG temperature sensors help to locate groundwater leakage in dams [21], pipelines [22] or coal mines [23]. CFBG systems are currently mostly applied for distributed strain measurements [24], rarely for distributed temperature measurements [25,26].

Several review papers have been published comparing the performance of distributed and multiplexed fiber optic sensors for hydrological applications [27,11,28]. Still, in no study different fibers were used alongside each other in the same experiment. This paper presents a comparison of FBG, DTS, CFBG and resistance thermometers during a heat tracing experiment in a groundwater flow simulator. Homogeneous soil structure and constant flow allowed to study the effect of sensor mounting, packaging type and packaging thickness.

2. Materials and methods

2.1. Groundwater flow simulator and sensors

The performance of three types of fiber optic temperature sensors was evaluated under laboratory conditions with a heat tracing experiment in a groundwater flow simulator. The temperature of the inflow water was increased by 10 °C by mixing with hot water for a short period of time. The groundwater flow simulator used in this experiment was a tank of 1 m width, 2 m length, and 1 m height, filled with sand of an uniform grain size (Fig. 1). The inflow and outflow of the tank goes through six perforated tubes with 0.5 mm vertical slits. The flow is the result of a hydraulic head gradient between the inflow and the outflow container. The setup was used to create a constant flow with a velocity of 2.9 m d^{-1}. This was the average flow inside the entire tank, as inferred from mass balance.

Three fiber optic sensors were chosen for this experiment: distributed temperature sensing, fiber Bragg gratings, and continuous fiber Bragg grating. Two bundles of fiber optic sensors were placed in the groundwater flow simulator, labeled as bundle A and B. Location of all sensors is shown in Figs. 1 and 2 . Fiber optic sensors were attached to a frame to ensure their orientation perpendicular to the flow. The frame was built from hollow PVC tubes with a 5 cm diameter. DTS, FBG, CFBG sensing fibers, and PT100 probes were all bundled together using several tie wraps along the length. Fibers were pre-stretched to keep them vertical and taped to the frame. After the frame was placed in the tank, the tank was filled with water and manually with sand to ensure a homogeneous sand distribution. The top part was sealed with a clay layer. Further description of the experimental setup can be found in [29].

DTS, FBG and CFBG sensing fibers all had different packaging, see cross-sections in Fig. 3. The DTS sensing fiber consists of four standard telecom multimode optical fibers (two looped fibers, one is a backup in case one breaks) with a thick PVC isolation. The fibers have a core diameter of 62.5 μm and a cladding diameter of 125 μm. This sensing fiber also contains a layer with metal wires and can be used in active heating experiments. The total thickness of DTS sensing fiber is 7.5 mm (LEONI Fiber Optics, Foeritztal, Germany).

FBG and CFBG packaging consists of loosely fitting tubes intended to isolate the optical fibers from strain effects. Two types of FBG packaging were used – a Teflon tube and a PVC tube, both with 3 mm diameter. The FBG sensors were written through the acrylate coating in the Corning SMF-28 single mode optical fiber with a core diameter of 9 μm and a cladding diameter of 125 μm (FemtoFiberTech, Germany). Teflon-packaged fibers had FBG sensors uniformly spaced by 10 cm with Bragg wavelengths of 1527, 1536, 1545, 1554, 1563 and 1572 nm. The length of each grating was 4 mm, reflectivity was around 65% and the bandwidth of sensors was 0.37 nm. These sensors were apodized. PVC-packaged fibers had FBG sensors uniformly spaced by 15 cm with Bragg wavelengths of 1527, 1536, 1545 and 1554 nm. The length of each grating was 2.5 mm, reflectivity was around 50% and the bandwidth of sensors was 0.33 nm.

The CFBG fiber was packaged in a steel tube with a 1.25 mm diameter. The CFBG sensing fiber is a single mode optical fiber with the same dimensions as FBG fibers. Refractive index in the core is modulated with a period of 2.6 mm along the entire length of the fiber, 15 m (LUNA, Roanoke, USA).

The PT100 probes (3-wire, Conrad) consist of a 6 cm steel packaging protecting the platinum wires.

2.2. Data processing and calibration

The PT100 data was collected with an Ecograph RSG30 (Endress+Hauser, Reinach, Switzerland) unit with a sampling period of 1 s.

The DTS data was collected with a DTS interrogator (Silixa Ultima, Silixa, London, UK). The data was collected for 15 s per channel at a spatial sampling interval of 12.5 cm. Each DTS data point is a 15 s average. The temperature along the length z was calculated from the measured power ratio of Stokes $P_S(z)$ and Anti-Stokes signal $P_{AS}(z)$:

$$T(z) = \frac{\gamma}{\ln \frac{P_S(z)}{P_{AS}(z)} + C - \Delta A z} \quad (2)$$

where γ (°C) represents an energy difference between incident and scattered photons, C (–) describes the differences in effective detec-

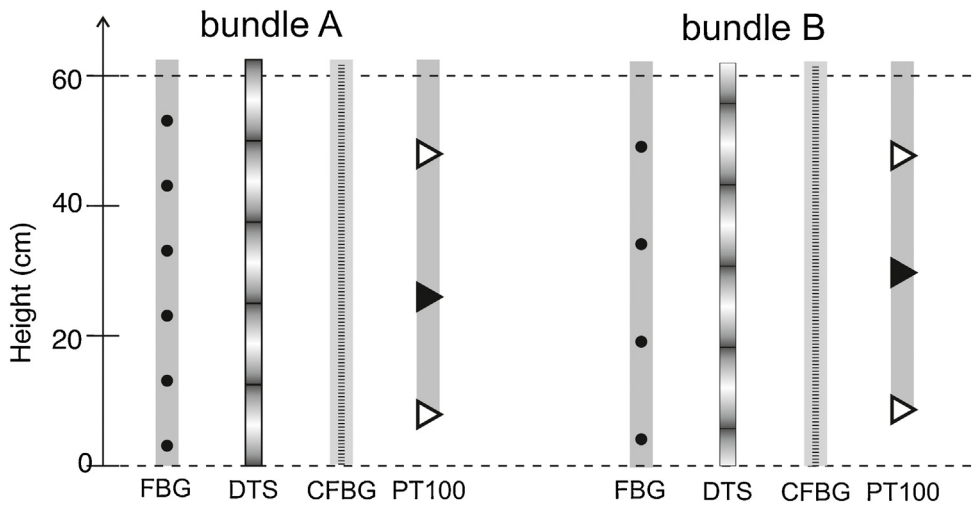

Fig. 2. Location of all sensors within fiber bundles. Dark circles indicate positions of the FBG sensors within the fiber. Black parts show DTS sampling points. The FBG, DTS, and CFBG data in the results were compared to the reference PT100 probes shown as ►.

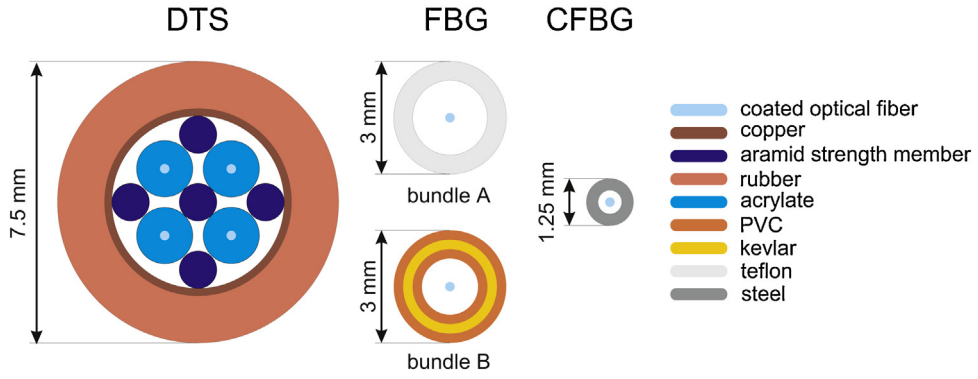

Fig. 3. Cross-sections of all fibers used in the groundwater flow simulator.

tor sensitivities with respect to Stokes and anti-Stokes photons and ΔA (m^{-1}) is the differential attenuation between the Stokes and anti-Stokes signal caused by light propagation along the optical fiber [30].

DTS data needs to be continuously calibrated during the measurement to get the calibration parameters γ, C, and ΔA. The DTS interrogator has an internal calibration mechanism consisting of a heated coil and an internal thermometer. However, the optical components of the DTS interrogator are temperature-sensitive [31], and this is why an external calibration was performed instead. The beginning and end of the DTS fiber was placed in a relatively warm and cold bath. The temperature of these baths was collected using PT100 sensors directly connected to the DTS interrogator. Calibration of the DTS data is based on the reference baths using a single-ended calibration method following Hausner et al. [32].

The FBG data was collected with an FBG interrogator (Gator, Technobis, Alkmaar, Netherlands) and optical switch (eol 1x16, LASER COMPONENTS GmbH, Olching, Germany), both controlled by a microcontroller (Raspberry Pi Model 3B, Raspberry Pi Foundation, Cambridge, UK). Every 20 s, 50 datasets were acquired at 1kHz frequency and averaged.

All FBG sensors used in this experiment were designed to have Bragg wavelengths in the range 1516-1584 nm of the interrogator's broadband LED source [33]. The interrogator determines the peaks of reflected wavelengths using a center-of-gravity algorithm. A shift in the reflected wavelength $\Delta\lambda$ with respect to the initial Bragg wavelength λ_{B0} is related to a temperature change ΔT and a strain change $\Delta\epsilon$ as:

$$\frac{\Delta\lambda}{\lambda_{B0}} = \alpha_T \Delta T + \alpha_\epsilon \Delta\epsilon \tag{3}$$

where α_T and α_ϵ are temperature and strain sensitivity coefficients. α_T has two components:

$$\alpha_T = \alpha_n + \alpha_\Lambda \tag{4}$$

α_n is a thermo-optic coefficient which describes the change of refractive index due to temperature, and α_Λ is a thermal expansion coefficient describing the change of the grating length due to temperature. For this heat tracing experiment, strain effects were assumed to be negligible. α_T was calculated from a calibration in a hot bath, where FBG fiber was strain-free. During the calibration, water in the bath is heated by a known temperature difference ΔT while measuring Bragg wavelengths λ_B. The temperature ΔT was acquired for both FBG and CFBG using NTC thermistors (TSP01, Thorlabs). For FBG, eight sensors per fiber were used to get an average value of α_T for each packaging type.

α_T does not change during the experiment, so this calibration needs to be performed only once. However, if an FBG interrogator does not have an internal wavelength reference, a wavelength drift introduces an error in the measurement. To correct for long-term wavelength drift, the FBG interrogator was combined with an external temperature-controlled FBG sensor (ITC4005, Thorlabs, Newton, MA, USA). Wavelength drift measured at the reference FBG sensor $\Delta\lambda_{ref}$ was subtracted from wavelength shift measured at

other FBG sensors, and temperature change was calculated using a method by [34]:

$$\Delta T = \frac{1}{\alpha_T} \cdot \left(\frac{\Delta\lambda}{\lambda_{B0}} - \frac{\lambda_{B0}\Delta\lambda_{ref}}{\lambda^2_{ref0}} \right) \quad (5)$$

Data from the CFBG fiber was collected with a CFBG interrogator (ODiSI-B, LUNA, Roanoke, USA) using the Coherent Rayleigh Optical Time Domain Reflectometry (COTDR) method [35]. At first, a reference reflection spectrum is acquired along the entire fiber length, called the 'tare' spectrum. The interrogator continuously records changes in the reflection spectrum caused by temperature and strain:

$$\frac{\Delta f}{f_{B0}} = \alpha_T \Delta T + \alpha_\epsilon \Delta\epsilon \quad (6)$$

The frequency shift Δf is calculated by cross-correlating the reflection spectrum with the reference spectrum. The CFBG fiber constitutes one arm of a Mach–Zehnder interferometer, so the intensity modulation of the reflected light contains information about the time delay and can be translated into position along the fiber. The interrogator contains a swept wavelength source in the range 1510–1570 nm and the initial Bragg wavelength of the CFBG grating is 1550 nm (f_{B0} = 193 THz) [36]. CFBG data were additionally scaled down by a factor of 2, which was most likely introduced during the definition of the sensor and has no physical meaning.

α_T can be calculated from a one-time calibration in a hot bath, in the same way as for FBG sensors. The resulting value is an average from a 25 cm section of the CFBG fiber in a hot bath.

2.3. Compared specifications of the fiber optic sensors

2.3.1. Spatial resolution

The spatial resolution of DTS measurements depends on the sensitivity of DTS interrogator and thermal properties of the optical fiber [37]. The value is generally 2–10 times larger than the spatial sampling interval at which the DTS data is collected [38]. Spatial resolution needs to be calculated for each application because it might significantly differ for field and laboratory experiments. There is no standard method how to define and calculate DTS spatial resolution [37]. The most common method, also used in this paper, is called the 90% step change. The DTS fiber was placed in a hot bath to observe step temperature change in the fiber. The spatial resolution is defined as the minimum length of the fiber required to detect 90% of the step change in the signal as described in [39]. The value is affected by thermal conductivity of the fiber and packaging – the packaging with higher thermal conductivity coefficient will increase the length of the step change.

The spatial resolution of FBG sensors is given by the physical spacing of the sensors, they are point temperature sensors.

In case of distributed CFBG sensor, the spatial resolution is defined as a length of the fiber used to calculate a single temperature measurement. It equals twice the value of the grating period [36].

2.3.2. Temperature resolution

The temperature resolution for the DTS is given by the resolution of the temperature probes used during the calibration.

The temperature resolution for the FBG and CFBG $R_{(C)FBG}$ was calculated as the temperature change per wavelength change $\Delta\lambda$ of 1 pm (resolution of the spectrometer in the interrogators) at λ_{B0} = 1550 nm:

$$R_{(C)FBG} = \Delta T = \frac{\Delta\lambda}{\alpha_T \lambda_{B0}} \quad (7)$$

Table 1
Temperature sensitivity coefficients for different types of packaging.

	FBG		CFBG
	Teflon	PVC	steel
$\alpha_T \pm \sigma$ (°C^{-1})	$(7.43 \pm 0.26) \times 10^{-6}$	$(6.91 \pm 0.24) \times 10^{-6}$	$(9.32 \pm 0.3) \times 10^{-6}$

2.3.3. Accuracy

The DTS accuracy is given and limited by the accuracy of the calibration probes. Since DTS needs a continuous calibration to get correct absolute temperature values, the accuracy for DTS was calculated as a Root mean square error (RMSE) during the entire duration of the measurement:

$$A_{DTS} = \sqrt{\frac{\sum_{i=1}^{n}(T_{DTS} - T_{cal})^2}{n}} \quad (8)$$

where T_{DTS} is the temperature measured by DTS and T_{cal} isthe temperature measured by calibration probes, n is a number of time points to average. The measurement interval was 9 h. The temperature from calibration probes was smoothed using a 10 min moving average filter to improve the calibration.

The calculated ΔT for the FBG and CFBG depends on the temperature sensitivity coefficient α_T. Therefore, (C)FBG accuracy depends on accuracy of the α_T calculation. When α_T changes by a standard deviation σ, (C)FBG will measure a temperature change $\Delta T'$:

$$\Delta T' = \frac{\alpha_T}{\alpha_T + \sigma} \Delta T \quad (9)$$

Accuracy $A_{(C)FBG}$ for a given ΔT can be calculated as a difference between $\Delta T'$ and ΔT:

$$A_{(C)FBG} = \Delta T' - \Delta T = \left(\frac{\alpha_T}{\alpha_T + \sigma} - 1 \right) \Delta T \quad (10)$$

3. Results and discussion

Specifications of compared fiber optic sensors were calculated from calibration experiments and are listed in Tables 1 and 2 .

All data were linearly interpolated with a time step of 1 min and a height step of 1 cm to visualize heat propagation in the sand. Since the spatial resolution for different fiber optic sensors was different, linear interpolation was needed to compare relative temperature profiles ΔT at the same height. The presented heat maps are from the middle section of the groundwater flow simulator, where the flow was expected to be laminar and not affected by preferential flow along horizontal parts of the PVC frame.

3.1. Spatial resolution

The heat maps in Fig. 4 were created to visualize heat convection through the groundwater flow simulator. As can be seen from the FBG and CFBG heat maps, the thermal plume has a parabolic shape in the vertical direction, which confirms the laminar flow assumption in the chosen section of the groundwater flow simulator. The laminar profile is not apparent in the DTS heat maps, because the DTS data is spatially averaged over a 1 m interval. Data from all sampling points only slightly differs due to the noise. The FBG spatial resolution of 10 and 15 cm combined with a linear interpolation was sufficient to show temperature changes in the vertical direction. The CFBG spatial resolution of 5.2 mm is unnecessarily high for this particular experiment.

High spatial resolution creates heavy requirements on data storage and processing; therefore it is better to customize the resolution to the intended application. FBG sensors offer this possibility because the user chooses the physical distance between the sensors in the fiber. Spacing of the sensors can be also irregular, which

Table 2
Comparison of PT100 and fiber optic temperature sensors. All values for the PT100 probes were taken from a manual of the data unit [40], DTS resolution was taken from [41]. Other values were calculated as described in Section 2.3. The last row tells if strain effects were observed for a particular sensing fiber.

Sensors	PT100	DTS	FBG		CFBG
			Bundle A	Bundle B	
Sampling period (s)	1	93	20		1.2
Spatial resolution (cm)	–	100	10	15	0.52
Temperature resolution (°C)	0.01	0.01	0.09	0.09	0.07
Accuracy for $\Delta T = 6$ °C (±°C)	1.1	0.24	0.22	0.22	0.2
Strain effects	No	No	Yes	No	Yes

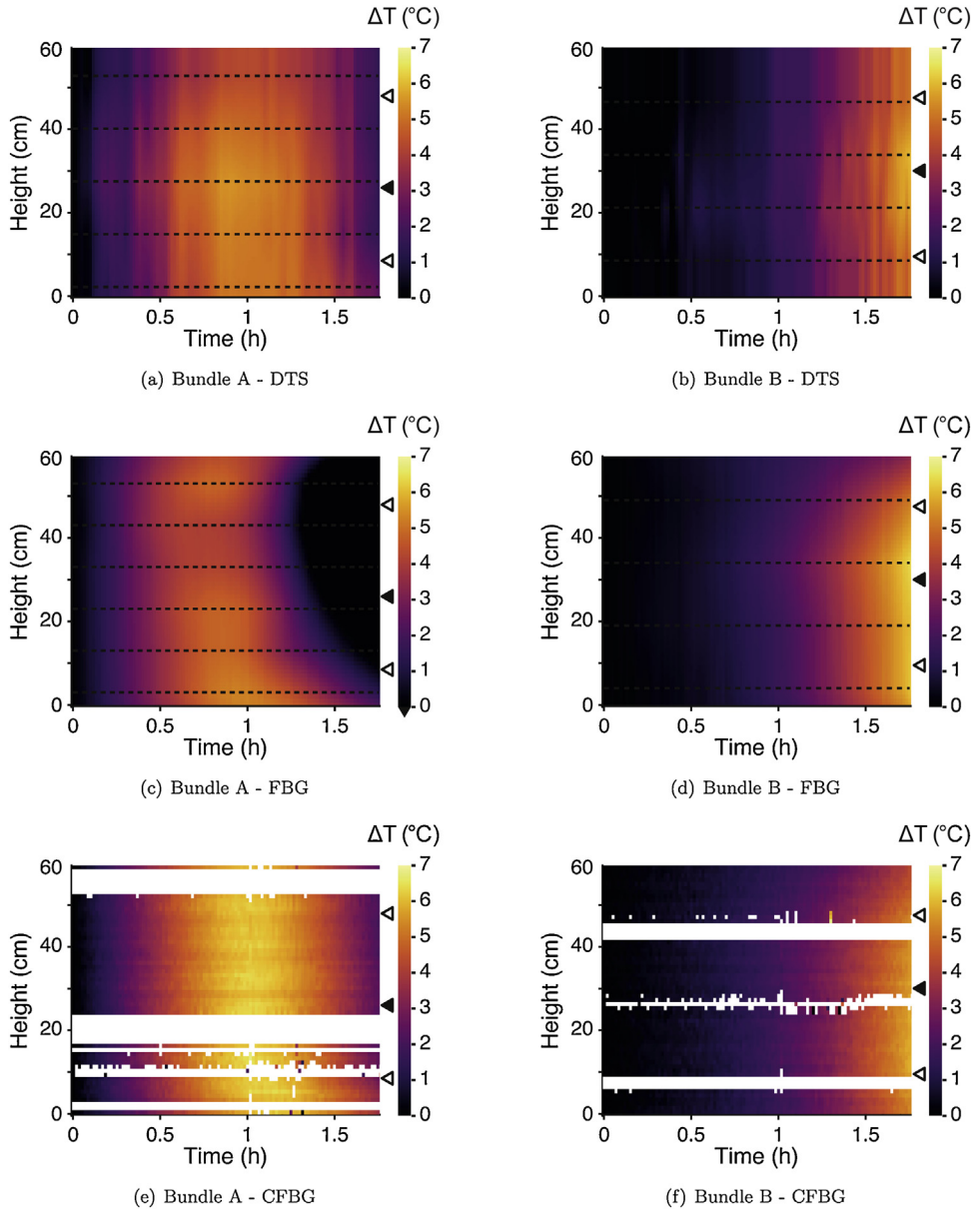

Fig. 4. Interpolated heat maps from temperature data measured by three types of fiber optic sensors. Blacked dashed lines show the location of fiber optic sensors, ▷ are PT100 probes, data from PT100 probes marked as ▶ are used for comparison with fiber optic sensors. ▷ and ▶ indicate the location of PT100 mid-points. White areas in (e) and (f) are data outside of the range indicated on the colorbar. (For interpretation of the references to color in this figure legend, the reader is referred to the web version of this article.)

allows to focus only on the regions of the interest. CFBG data can be spatially downsampled. The spatial resolution of DTS can be increased by coiling the fiber around rods or conduits, however, this construction introduces signal attenuation and temperature deviations [40]. Coiled fibers also create an obstacle to the flow in small scale setups. Under field conditions DTS technology can also be customized by choosing smaller spatial resolution in the software.

For FBG and CFBG, spatial resolution is related to the price of the sensing fiber. The price of the FBG fiber depends on the num-

ber of sensors inside. CFBG with a high spatial resolution is more expensive to fabricate. DTS fiber is usually the cheapest because it does not need any modifications to the standard telecom fiber. In our case, DTS fiber was the cheapest and CFBG fiber the most expensive one.

The spatial resolution for each fiber optic sensor should be chosen in such a way to capture heterogeneity of the investigated site. If variation of soil properties is unknown, it is better to choose a distributed sensor to get more data along the entire length of the fiber. High spatial resolution is needed to study heat propagation or flow in heterogeneous groundwater environments and boundary effects between soil layers. Distributed sensors give more spatial information along the entire length, while multiplexed sensors can better show local anomalies.

The spatial resolution of DTS, 1 m, is sufficient for most of the field applications. Since the DTS sensing fiber is also cheaper than FBG or CFBG fiber, DTS is well suited for groundwater heat tracing experiments, for example to measure flow or thermal interference between wells of ATES systems. FBG and CFBG fibers with higher spatial resolution than DTS are more suitable choice for environments like muddy deposits or areas with soil layer boundaries. Using FBG and CFBG sensors also allows to downscale the simulated setups for investigating subsurface processes. Some examples of these processes are temperature-induced buoyancy or migration of pollutants due to changing temperature.

3.2. Temperature resolution and accuracy

DTS has the best temperature resolution of all the examined fiber optic technologies, given by the calibration PT100 probes. However, as visible from Fig. 5, DTS data is also quite noisy. To be able to see temperature differences of 0.01 °C, DTS data needs more averaging. The temperature resolution of the FBG and CFG sensors is worse than the resolution of commercially available PT100 probes. The temperature resolution of FBG-based fiber optic technologies can be improved by embedding the sensors in a packaging material with a thermal expansion coefficient higher than a thermal expansion coefficient for glass [41].

For this small temperature change ($\Delta T = 6\,^{\circ}\mathrm{C}$), all fiber optic sensor have a comparable relative accuracy of the measurements. Their accuracy is better than accuracy of the PT100 probes. PT100 connected in a 3-wire configuration can introduce a constant offset due to differences in wire resistance. DTS accuracy can be improved by mixing water in the calibration baths to have more uniform temperature for submerged sections. The accuracy of (C)FBG can possibly be increased by more repetitions of the calibration experiment, reducing the standard deviation of α_T values. DTS needs a continuous calibration to keep the accuracy while FBG and CFG need to be calibrated once.

Fiber optic technologies are graphically compared to PT100 probes in Fig. 5. In bundle A, DTS and CFBG give similar temperature curves which differ from the measured PT100 curve during the temperature increase. The DTS curve misses the sharp peak at $t = 1$ h which might be caused by the presence of the noise. PT100 probes sometimes overestimate the real temperature if the temperature gradient is large. The results indicate that this PT100 probe needs to be recalibrated. The FBG from bundle A is most likely affected by strain effects because temperature in the groundwater simulator did not decay as fast as FBG data shows. All sensors in bundle B measure similar temperature profiles, and the FBG is the closest one to the PT100 probe.

It is not possible to say which sensor is ideal for this laboratory experiment, all tested sensors have their advantages and disadvantages. All tested fiber optic temperature sensors have sufficient accuracy and resolution for groundwater temperature measurements. For leakage detection it is important that the sensor responds fast. It does not need to be very accurate, as long as it shows a step change in temperature. For long term groundwater temperature monitoring the sensors do need high accuracy and resolution. In case of DTS this involves extra effort to ensure stability by continuous calibration using temperature baths. The accuracy of FBG and CFBG measurements is stable over a long period and only deviates when the coating deteriorates. Higher accuracy would allow for detection of smaller groundwater flow velocities using the active heat tracing method [29].

3.3. Strain effects

Strain might cause a response of (C)FBG sensors. Three different types of packaging were designed to minimize strain effects. However, strain effects are still visible in Fig. 4(c), (e), and (f). We expect that strain was introduced by mounting of the sensing fibers on the frame.

The shape of the thermal plume in Fig. 4(c) is asymmetric with respect to the height and also time. Comparison of FBG images with the other fiber optic sensors shows that the deformation of the thermal plus is located in the section from 20 to 60 cm. The affected section of the fiber is located between two tie wraps, creating strong pressure points. The tie wraps pre-stretched a section of the FBG fiber during installation, and we expect that this strain was slowly released during the experiment, resulting in a negative wavelength shift, translating to a negative temperature. Relative temperature profiles in Fig. 5(a) show that strain effects cause an FBG response on the same order of magnitude as the temperature. Strain effects are not visible for the FBG fiber of bundle B.

The CFBG fibers inside the metal tube are affected by strain at several locations along the length. Some CFBG data translated to temperature was so far outside the expected scale −1000 up to 1000 °C that it was automatically removed by the data collection software, see the white spots in Fig. 4(e) and (f). The wavelength shift at these sections is $\pm 1 \times 10^4$ pm, while temperature changes in the other sections along the length are $< 1 \times 10^2$ pm, which makes the strain effects two orders of magnitude larger than temperature effects. The location of the strain effects along the CFBG fiber corresponds to the location of tie wraps. Apparently, tie wraps locally pressure the CFBG fiber against the rigid metal wall and stretch the grating. Each PT100 probe was attached to the fiber bundle with a tie wrap, so the strain effects are present near their location (see ► and ▷ on the right side of CFBG heat maps). Even though the tie wraps were as wide as 3 mm, the length affected by strain is an interval up to 7 cm around each tie wrap.

FBG fibers can be used for measuring temperature in both laboratory and field setups, but one needs to be careful not to introduce pre-strain. Strain effects introduced by attaching the FBG fibers to a frame can easily reach the same order as temperature effects, and then it is difficult to separate both effects. These effects can be avoided, as seen in Fig. 5(b). In the field conditions, fibers should be loosely packed in soil and should not have heavy objects attached to it.

3.4. Effect of the packaging

All sensor types need to be calibrated to include the effect of packaging in the temperature sensitivity coefficient. For DTS, the material and thickness of the packaging do not influence the accuracy of the measured temperature because DTS is continuously calibrated. However, if the packaging is very thick it isolates the optical fiber and measured intensities do not rise above the noise. FBG and CFBG need to be calibrated once, α_T depends on the packaging material, not on the thickness. According to Table 1, steel has the highest coefficient. This high coefficient value can be attributed to differences in thermo-optic coefficient α_n between

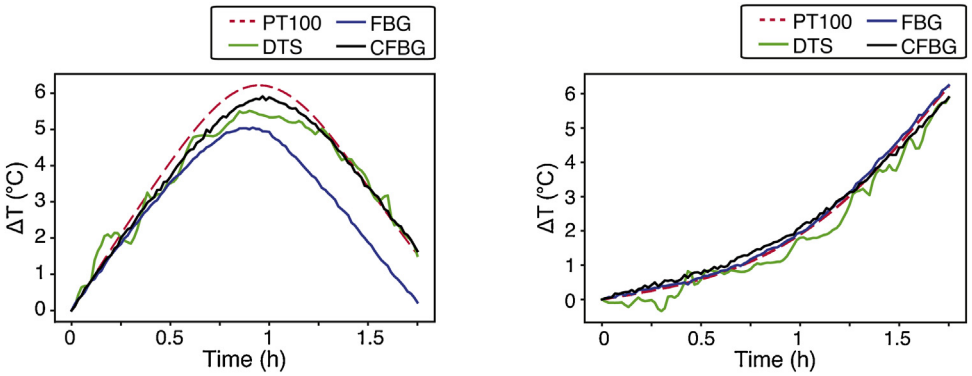

Fig. 5. Relative temperature measured by fiber optic sensors and reference PT100 probes (marked as ▶ in Fig. 4). Since reference PT100 probes are 6 cm long, the displayed temperature curves are also 6 cm averages from (a) 26 ± 3 cm and (b) 30 ± 3 cm.

CFBG and FBG fibers, and not directly to the high thermal expansion coefficient α_Λ of steel. CFBG fiber has most likely higher thermo-optic coefficient because it was doped more to increase its photosensitivity and allow more accurate writing of the long grating [42].

Packaging also introduces a delay in the temperature measured by (C)FBG compared to the temperature of the sand-water mixture. This delay is not visible for FBG and CFBG fibers in Fig. 5. The sensing fibers reach the environmental temperature roughly as quickly as PT100 probes, and 1 mm-thick packaging does not seem to influence the temperature measurement.

For the metal tube of CFBG and the metal wires in the DTS cable, it was assumed that heat might propagate along the packaging and create a spatial averaging effect. This effect is not apparent from any CFBG or DTS heat maps, likely because in this experiment temperature gradient along the height was negligible and DTS spatial resolution is not sufficient. We still think that metal packaging is not suitable for experiments with spatial temperature gradients. This considerably restricts its applicability for temperature measurements and we recommend choosing a plastic packaging instead.

Moreover, metal packaging is not very suitable for laboratory experiments because it is difficult to bend to the desired shape. Changing the shape of the metal tube using tie wraps introduces significant strain effects. It is possible that the strain effects would also appear in the field experiments if the metal tube is not straight when it is packed by heavy soil material.

4. Conclusion

There are many types of optical fiber sensors capable of measuring temperature in hydrological applications. The choice can be made based on their spatial sampling intervals, sampling frequency or price, but their accuracy and resolution has to be determined from an experimental calibration. Other factor which matters when choosing a fiber optic temperature sensor is how much error is introduced by the sensor placement technique, packaging, or cross-sensitivity between temperature and strain. These errors were analyzed in laboratory conditions during a heat tracing experiment in a groundwater simulator. Accuracy and temperature resolution of three commercially available fiber optic sensors were determined and compared with reference PT100 probes. The tested sensors were distributed temperature sensors, fiber Bragg gratings and continuous fiber Bragg grating.

In terms of spatial resolution, the FBG sensors were the most suitable for the experiment because distance between the sensors was chosen based on the setup dimensions. CFBG sensors were suitable as well. DTS is not suitable for this experiment because spatial resolution of 1 m [27] is insufficient for the small scale setup like applied here.

Fiber optic sensors need to be calibrated with conventional temperature probes which limits their accuracy and resolution. All tested fiber optic sensors have a comparable accuracy, ≈0.2 °C, better than the accuracy of PT100 probes used during the experiment. The results also showed that one PT100 probe needs to be recalibrated. DTS has the best temperature resolution, however, to reach this resolution, DTS data collected with 93 s period needs more temporal averaging. This accuracy and resolution can be achieved when DTS fibers are continuously calibrated during the experiment. FBG and CFBG fibers need one-time calibration, but unlike DTS, only relative temperature changes can be measured.

DTS measures only temperature and is insensitive to strain effects, which means that the installation of the fibers does not affect the sensor performance. FBG and CFBG sensors can be used for measuring temperature as long as the strain effects are eliminated. Even if fibers are in a loose tube, strain effects can still be introduced by pre-stretching the fibers or firmly attaching them with tie wraps. To avoid strain effects during fiber installation in soil, fibers need to be loosely packed. Fiber packaging also influences the temperature sensitivity of the sensors. The thickness of the packaging did not have a visible effect on the performance of the sensors.

Calibration of fiber optic sensors with thermometers or thermistors currently cannot be avoided. However, fiber optic technologies can also be combined and calibrate each other during the measurement. Once FBG or CFBG are calibrated, they can be used as a reference for DTS and eliminate the need for continuous calibration during the measurement. Alternatively, DTS can be used to measure absolute temperature and add an offset to (C)FBG measurements or identify strain effects in the (C)FBG data.

Authors' contribution

Sandra Drusová: conceptualization, methodology, software, validation, formal analysis, investigation, data curation, writing – original draft, writing – review & editing, visualization. Wiecher Bakx: conceptualization, methodology, software, formal analysis, investigation, data curation, writing – review & editing. Pieter J. Doornenbal: conceptualization, methodology, software, investigation, resources, writing – review & editing, supervision, project administration. R. Martijn Wagterveld and Herman L. Offerhaus: conceptualization, writing – review & editing, supervision. Victor F. Bense: writing – review & editing.

Funding

Wetsus is co-funded by the Dutch Ministry of Economic Affairs and Ministry of Infrastructure and Environment, the Province of Fryslân, andthe Northern Netherlands Provinces. This research received funding from the European Union's Horizon 2020 research and innovation programme under the Marie Skłodowska-Curie grant agreement no. 665874.

Declaration of Competing Interest

The authors report no declarations of interest.

Acknowledgements

This work was performed in the cooperation framework of Wetsus, European Centre of Excellence for Sustainable Water Technology (www.wetsus.nl). We are grateful to the participants of the research theme "Groundwater technology" for fruitful discussions and financial support. We also wish to express our gratitude to Deltares without whose personnel, equipment, and location support this experiment would not have been possible.

Appendix A. Supplementary data

Supplementary data associated with this article can be found, in the online version, at https://doi.org/10.1016/j.sna.2021.112682.

References

[1] M.P. Anderson, Heat as a ground water tracer, Ground Water 43 (6) (2005) 951–968, http://dx.doi.org/10.1111/j.1745-6584.2005.00052.x, ISSN 0017467X.
[2] R. Ma, C. Zheng, Effects of density and viscosity in modeling heat as a groundwater tracer, Ground Water 48 (3) (2010) 380–389, http://dx.doi.org/10.1111/j.1745-6584.2009.00660.x, ISSN 0017467X.
[3] M. Bonte, B.M. van Breukelen, P.J. Stuyfzand, Temperature-induced impacts on groundwater quality and arsenic mobility in anoxic aquifer sediments used for both drinking water and shallow geothermal energy production, Water Res. 47 (14) (2013) 5088–5100, http://dx.doi.org/10.1016/j.watres.2013.05.049, ISSN 18792448.
[4] T. Saito, S. Hamamoto, T. Ueki, S. Ohkubo, P. Moldrup, K. Kawamoto, T. Komatsu, Temperature change affected groundwater quality in a confined marine aquifer during long-term heating and cooling, Water Res. 94 (2016) (2016) 120–127, http://dx.doi.org/10.1016/j.watres.2016.01.043, ISSN 18792448.
[5] V.F. Bense, B.L. Kurylyk, J. van Daal, M.J. van der Ploeg, S.K. Carey, Interpreting repeated temperature-depth profiles for groundwater flow, Water Resour. Res. 53 (10) (2017) 8639–8647, http://dx.doi.org/10.1002/2017WR021496, ISSN 19447973.
[6] M.A. Briggs, L.K. Lautz, J.M. Mckenzie, A comparison of fibre-optic distributed temperature sensing to traditional methods of evaluating groundwater inflow to streams, Hydrol. Process. 26 (9) (2012) 1277–1290, http://dx.doi.org/10.1002/hyp.8200, ISSN 08856087.
[7] T. Read, O. Bour, V. Bense, T. Le Borgne, P. Goderniaux, M.V. Klepikova, R. Hochreutener, N. Lavenant, V. Boschero, Characterizing groundwater flow and heat transport in fractured rock using fiber-optic distributed temperature sensing, Geophys. Res. Lett. 40 (10) (2013) 2055–2059, http://dx.doi.org/10.1002/grl.50397, ISSN 00948276.
[8] M. Bloemendal, T. Olsthoorn, ATES systems in aquifers with high ambient groundwater flow velocity, Geothermics 75 (2018) 81–92, http://dx.doi.org/10.1016/j.geothermics.2018.04.005, ISSN 03756505.
[9] R.E. Sweeney, G. Todd Ririe, Temperature as a tool to evaluate aerobic biodegradation in hydrocarbon contaminated soil, Groundwater Monit. Remed. 34 (3) (2014) 41–50, http://dx.doi.org/10.1111/gwmr.12064, ISSN 17456592.
[10] R. Hajovsky, S. Ozana, Long term temperature monitoring and thermal processes prediction within mining dumps, Proceedings of the 6th IEEE International Conference on Intelligent Data Acquisition and Advanced Computing Systems: Technology and Applications, IDAACS'2011, vol. 2 (August 2015) (2011) 522–526, http://dx.doi.org/10.1109/IDAACS.2011.6072821.
[11] J.S. Selker, L. Thévenaz, H. Huwald, A. Mallet, W. Luxemburg, N. Van De Giesen, M. Stejskal, J. Zeman, M. Westhoff, M.B. Parlange, Distributed fiber-optic temperature sensing for hydrologic systems, Water Resour. Res. 42 (12) (2006) 10040, http://dx.doi.org/10.1029/2006WR005326, ISSN 00431397.
[12] R. Engelbrecht, Fiber Optic strain and temperature sensing: overview of principles, AMA Conferences 2017 (2017) 255–260, http://dx.doi.org/10.5162/sensor2017/B6.1.
[13] R. Kashyap, Fiber Bragg Gratings. Electronics & Electrical, Elsevier Science, 1999, ISBN 9780124005600. https://books.google.nl/books?id=tv2AMFhwB4wC.
[14] A. Ukil, H. Braendle, P. Krippner, Distributed temperature sensing: review of technology and applications, IEEE Sens. J. 12 (5) (2012) 885–892, http://dx.doi.org/10.1109/JSEN.2011.2162060, ISSN 1530-437X.
[15] V.P. Kaandorp, P.J. Doornenbal, H. Kooi, H. Peter Broers, P.G.B. de Louw, Temperature buffering by groundwater in ecologically valuable lowland streams under current and future climate conditions, J. Hydrol. X 3 (2019) 100031, http://dx.doi.org/10.1016/j.hydroa.2019.100031, ISSN 25899155.
[16] M.A. Briggs, S.F. Buckley, A.C. Bagtzoglou, D.D. Werkema, J.W. Lane, Actively heated high-resolution fiber-optic-distributed temperature sensing to quantify streambed flow dynamics in zones of strong groundwater upwelling, Water Resour. Res. 52 (7) (2016) 5179–5194, http://dx.doi.org/10.1002/2015WR018219, ISSN 19447973.
[17] T. Read, V.F. Bense, R. Hochreutener, O. Bour, T. Le Borgne, N. Lavenant, J.S. Selker, Thermal-plume fibre optic tracking (T-POT) test for flow velocity measurement in groundwater boreholes, Geosci. Instrum. Methods Data Syst. 4 (2) (2015) 197–202, http://dx.doi.org/10.5194/gi-4-197-2015, ISSN 21930864.
[18] S.M. Sellwood, D.J. Hart, J.M. Bahr, An in-well heat-tracer-test method for evaluating borehole flow conditions, Hydrogeol. J. 23 (8) (2015) 1817–1830, http://dx.doi.org/10.1007/s10040-015-1304-8, ISSN 1431-2174.
[19] F. Selker, J.S. Selker, Investigating water movement within and near wells using active point heating and fiber optic distributed temperature sensing, Sensors (Switzerland) 18 (4) (2018) 1–14, http://dx.doi.org/10.3390/s18041023, ISSN 14248220.
[20] B.F. des Tombe, M. Bakker, F. Smits, F. Schaars, K.J. van der Made, Estimation of the variation in specific discharge over large depth using distributed temperature sensing (DTS) measurements of the heat pulse response, Water Resour. Res. 55 (1) (2019) 811–826, http://dx.doi.org/10.1029/2018WR024171, ISSN 19447973.
[21] J. Chen, J. Zheng, F. Xiong, Q. Ge, Q. Yan, F. Cheng, Experimental investigation of leak detection using mobile distributed monitoring system, Smart Mater. Struct. 27 (1) (2017) 015025, http://dx.doi.org/10.1088/1361-665x/aa9c78.
[22] S.I. Jahnke, Pipeline Leak Detection Using In-Situ Soil Temperature and Strain Measurements (Ph.D. thesis), University of Pretoria, 2018 https://www.up.ac.za/media/shared/124/ZP_Resources/JahnkeMEng.pdf.
[23] B. Liu, S.C. Li, J. Wang, Q.M. Sui, L.C. Nie, Z.F. Wang, Multiplexed FBG monitoring system for forecasting coalmine water inrush disaster, Adv. OptoElectron. (2012), http://dx.doi.org/10.1155/2012/895723, ISSN 1687563X.
[24] L. Schenato, L. Palmieri, M. Camporese, S. Bersan, S. Cola, A. Pasuto, A. Galtarossa, P. Salandin, P. Simonini, Distributed optical fibre sensing for early detection of shallow landslides triggering, Sci. Rep. 7 (1) (2017) 2–5, http://dx.doi.org/10.1038/s41598-017-12610-1, ISSN 20452322.
[25] J. Drahotský, P. Hanzelka, V. Musilová, M. Macek, R. du Puits, P. Urban, Temperature profiles measurements in turbulent Rayleigh-Bénard convection by optical fibre system at the Barrel of II-menau, EPJ Web Conf. 180 (2018) 02020, http://dx.doi.org/10.1051/epjconf/201818002020.
[26] X. Lu, M.A. Soto, L. Thévenaz, MilliKelvin resolution in cryogenic temperature distributed fibre sensing based on coherent Rayleigh scattering, 23rd International Conference on Optical Fibre Sensors, 9157:91573R (2014), http://dx.doi.org/10.1117/12.2059659, ISSN 1996756X.
[27] P. Lu, N. Lalam, M. Badar, B. Liu, B.T. Chorpening, M.P. Buric, P.R. Ohodnicki, Distributed optical fiber sensing: review and perspective, Appl. Phys. Rev. 6 (4) (2019), http://dx.doi.org/10.1063/1.5113955, ISSN 19319401.
[28] L. Schenato, A review of distributed fibre optic sensors for geo-hydrological applications, Appl. Sci. 7 (9) (2017), http://dx.doi.org/10.3390/app7090896, ISSN 20763417.
[29] W. Bakx, P.J. Doornenbal, R.J. van Weesep, V.F. Bense, G.H.P. Oude Essink, M.F.P. Bierkens, Determining the relation between groundwater flow velocities and measured temperature differences using active heating-distributed temperature sensing, Water 11 (8) (2019) 1619, http://dx.doi.org/10.3390/w11081619.
[30] N. van de Giesen, S.C. Steele-Dunne, J. Jansen, O. Hoes, M.B. Hausner, S. Tyler, J. Selker, Double-ended calibration of fiber-optic raman spectra distributed temperature sensing data, Sensors (Switzerland) 12 (5) (2012) 5471–5485, http://dx.doi.org/10.3390/s120505471, ISSN 14248220.
[31] A. McDaniel, M. Harper, D. Fratta, J.M. Tinjum, C.Y. Choi, D.J. Hart, Dynamic calibration of a fiber-optic distributed temperature sensing network at a district-scale geothermal exchange borefield, Geo-Chicago 2016, number 270 (2016) 1–11, http://dx.doi.org/10.1061/9780784480137.001, ISBN 9780784480137.
[32] M.B. Hausner, F. Suárez, K.E. Glander, N. van de Giesen, J.S. Selker, S.W. Tyler, Calibrating single-ended fiber-optic Raman spectra distributed temperature sensing data, Sensors 11 (11) (2011) 10859–10879, http://dx.doi.org/10.3390/s111110859, ISSN 14248220.
[33] Gator User Manual, Technobis, Technobis Fibre Technologies, Pyrietstraat 2, 1812 SC Alkmaar, The Netherlands, 2016.
[34] S. Drusová, W. Bakx, A.D. Wexler, H.L. Offerhaus, Possibilities for groundwater flow sensing with fiber Bragg grating sensors, Sensors 19 (7) (2019), http://dx.doi.org/10.3390/s19071730, ISSN 1424-8220.

[35] Z. Yang, P. Shi, Y. Li, Research on COTDR for measuring distributed temperature and strain, 2nd International Conference on Mechanic Automation and Control Engineering, MACE 2011 – Proceedings, number 1 (2011) 590–593, http://dx.doi.org/10.1109/MACE.2011.5986993, ISBN 9781424494392.
[36] Optical Distributed Sensor Interrogator Model ODiSI-B: User's Guide, 2016.
[37] N. Simon, O. Bour, N. Lavenant, G. Porel, B. Nauleau, B. Pouladi, L. Longuevergne, A comparison of different methods to estimate the effective spatial resolution of FO-DTS measurements achieved during sandbox experiments, Sensors (Switzerland) 20 (2) (2020), http://dx.doi.org/10.3390/s20020570, ISSN 14248220.
[38] J.S. Selker, S. Tyler, N. van de Giesen, Comment on "Capabilities and limitations of tracing spatial temperature patterns by fiber-optic distributed temperature sensing" by Liliana Rose et al, Water Resour. Res. 50 (2014) 5372–5374, http://dx.doi.org/10.1002/2013WR014979.Received.
[39] S.W. Tyler, J.S. Selker, M.B. Hausner, C.E. Hatch, T. Torgersen, C.E. Thodal, S. SchladowGeoffrey, Environmental temperature sensing using Raman spectra DTS fiber-optic methods, Water Resour. Res. 46 (4) (2009) 1–11, http://dx.doi.org/10.1029/2008WR007052, ISSN 00431397.
[40] K. Hilgersom, T. Van Emmerik, A. Solcerova, W. Berghuijs, J. Selker, N. Van De Giesen, Practical considerations for enhanced-resolution coil-wrapped distributed temperature sensing, Geosci. Instrum. Methods Data Syst. 5 (1) (2016) 151–162, http://dx.doi.org/10.5194/gi-5-151-2016, ISSN 21930864.
[41] V. Mishra, M. Lohar, A. Amphawan, Improvement in temperature sensitivity of FBG by coating of different materials, Optik 127 (2) (2016) 825–828, http://dx.doi.org/10.1016/j.ijleo.2015.10.014, ISSN 00304026.
[42] Y.-J. Kim, U.-C. Paek, B. Ha Lee, Measurement of refractive-index variation with temperature by use of long-period fiber gratings, Opt. Lett. 27 (15) (2002) 1297, http://dx.doi.org/10.1364/ol.27.001297, ISSN 0146-9592.

Biography

Sandra Drusová received a master's degree from Palacký University Olomouc, Czechia, specializing in optics and optoelectronics. During her master's studies, she completed an internship at Wetsus, a water technology institute in the Netherlands. While at Wetsus she assisted in building an optical laboratory and researching properties of electrohydrodynamic bridges. It was during this time she realized she wanted to do research directly connected to industrial applications. In her master's thesis she developed a new method to check the surface quality of aspheric lenses. Shortly after graduating, she completed an internship at Sendai University in Japan, where she acquired more programming skills. In 2016 she began her PhD project at Wetsus in cooperation with the Optical Sciences department at University of Twente. She was intrigued with the challenges of developing a new optical sensor for a slow groundwater flow. She obtained her PhD degree in 2020. Her research interests include optical sensors and measurement methods.